Desalination and Water Treatment
www.deswater.com
doi: 10.1080/19443994.2015.1101021

57 (2016) 19216–19226
September

Taylor & Francis
Taylor & Francis Group

Preparation of iron oxide-based porous ceramsite from goethite and application for city wastewater treatment in biological aerated filters

Teng Bao[a,b], Tianhu Chen[a,*], Marie-Luise Wille[c], Xuehua Zou[a], Ray L. Frost[b], Chengsong Qing[a,d], Dong Chen[a,*]

[a]*Laboratory for Nanominerals and Environmental Material, School of Resource and Environmental Engineering, Hefei University of Technology, Hefei, China, email: tengbao1222@sina.com (T. Bao), Tel./Fax: +86 13956099615; emails: chentianhu@hfut.edu.cn (T. Chen), zouxuehu1988@163.com (X. Zou), csqing@hfut.edu.cn (C. Qing), Tel./Fax: +86 13955176245; email: cdxman@hfut.edu.cn (D. Chen)*

[b]*Science and Engineering Faculty, School of Chemistry, Physics and Mechanical Engineering, Queensland University of Technology, Brisbane, Australia, email: r.frost@qut.edu.au (R.L. Frost)*

[c]*Institute of Health & Biomedical Innovation, Queensland University of Technology, Brisbane, Australia, email: m.wille@qut.edu.au*

[d]*School of Material Science Chemical Engineering, Chu Zhou University, Chu zhou, China*

Received 16 February 2015; Accepted 21 September 2015

ABSTRACT

Ceramsite is a filter medium used in biological aerated filters (BAF). We prepared iron oxide-based porous ceramsite (IPC) by calcination in an O_2 atmosphere with goethite, sawdust, and palygorskite clay. The properties of the IPC were analyzed by X-ray diffraction (XRD), scanning electron microscope (SEM), thermal properties (TG), X-ray fluorescence (XRF), and porosimetry. Two kinds of IPC and commercial ceramsite (CC) were used in BAFs for the treatment of city wastewater. Goethite, sawdust, and palygorskite clay were used to produce IPC that was satisfactory for city wastewater treatment. IPC BAFs had average total organic carbon, P, TN, and NH_3-N removal rates of 67.92, 76.55, 43.15, and 90.71%, respectively, much better than those of CC BAFs. The uniform pore size in IPC, with its many interconnections, made it suitable for microbial growth. IPC appears suitable for use as a BAF ceramsite for simultaneous removal of nitrogen and phosphorus from city wastewater.

Keywords: Iron oxide-based porous ceramsite (IPC); Ceramsite; Palygorskite clay; Goethite; Biological aerated filter (BAF)

1. Introduction

Nitrogen and phosphorous compounds are nutrients essential for the growth of organisms in most ecosystems. An excessive amount of nitrogen and phosphorous from wastewater is found in many bodies of water, [1]. including Tai Lake, Chao Lake, and Dianchi Lake. This contamination is leading to a shortage of fresh water. The removal of nitrogen and phosphorus from wastewater has been the subject of widespread study for decades. Although a number of technologies have been applied, most of them are either too expensive or not yet available for full-scale use [2,3].

Conventional phosphate removal technologies include a combination of chemical and biological treatments [4–6]. The use of low cost and readily available natural nanomineral materials in wastewater has been

*Corresponding authors.

of particular interest. These materials include hematite, goethite, palygorskite clay, and nanoscale zero-valent iron [7–10]. Treatment with these materials has proven to be an effective method for the removal of phosphorus from wastewater.

Biological aerated filters (BAFs) have seen widespread use throughout the world in wastewater treatment systems because of their high removal efficiency of total nitrogen (TN), and ammonia nitrogen (NH_3-N) and improvements in chemical oxygen demand (COD) [11]. Biofilter carriers play an important role in maintaining active biomass and a variety of microbial populations [12–15]. Several new biofilter carriers have been developed for use in BAF systems to enhance their biodegradation capability [16–22]. Han et al. reported that sludge fly ash ceramic particles (SFCP) used in an up-flow lab-scale A/O BAF removed 90% of COD_{cr}, more than 98% NH_4^+-N, and approximately 70% TN from synthetic wastewater [23]. Liu et al. reported that an up-flow BAF packed with two layers of media increased dissolved oxygen (DO) concentrations from 2.4 to 6.1 mg/L and improved COD_{cr} and NH_4^+-N content from 39 to 53% and 64 to 88%, respectively, in the tertiary treatment of twice treated textile wastewater effluent [24]. Both biofilter carriers achieved good results for nitrogen removal. However, few reports have evaluated the simultaneous removal of nitrogen and phosphorus with BAFs.

Sawdust is the byproduct of timber processing. It has been reported that sawdust exposed to high sintering temperatures (≥400˚C) are converted into a carbonaceous porous material [25,26]. The formation of a porous network may improve microbial growth in IPC. We used sawdust as a pore-forming agent [3]. Palygorskite is an excellent absorbent and is used in many traditional applications [4]. Goethite is a stable crystalline iron oxyhydroxide, commonly encountered in nature, and therefore, it is very often used as a model solid for adsorption studies. During the sintering process, goethite is transformed into hematite in the presence of O_2 gas emitted during pyrolysis at 250–700˚C. It has been reported that hematite avidly absorbs phosphorus [10].

Dried sewage sludge sintering has been well studied [27,28]. However, the calcination of goethite, palygorskite clay, and sawdust in this process is not well studied. We evaluated the use of palygorskite clay, sawdust, and goethite in the fabrication of IPC for the removal of nitrogen and phosphorus from wastewater.

2. Materials and experimental procedure

2.1. Materials

Raw palygorskite clay was obtained from Crown Hill in Ming Guang City in China's Anhui Province. The sawdust was obtained from a wood-working factory in Hefei City, Anhui Province. Goethite was obtained from a fine chemical factory in Zhenjiang City, Jiangsu Province. The particle diameter of palygorskite clay, sawdust, and goethite after extrusion, and cutting and crushing was less than 0.074 mm. The compositions of the four raw materials are shown in Table 1.

2.2. Characterization

The multi-point BET (Brunauer, Emmett, and Teller) surface area of iron oxide-based porous ceramsite and commercial ceramsite (CC) was measured using a Quantachrome Nova 3000e automated surface

Table 1
Composition of raw materials (%)

Chemical composition of raw materials (wt%)							
	Sawdust (%)		Goethite (%)		Palygorskite (%)		Commercial ceramsite (%)
C	46.09	SiO_2	0.07	SiO_2	63.30	SiO_2	60.24
H	6.85	Al_2O_3	0.07	Al_2O_3	8.35	Al_2O_3	17.94
O	35.09	Fe_2O_3	99.23	Fe_2O_3	8.82	Fe_2O_3	13.16
N	0.60	P_2O_5	0.04	K_2O	1.17	K_2O	2.46
S	0.10	CaO	0.01	CaO	1.08	CaO	0.41
Cl	–	Cl	0.04	MgO	13.83	MgO	1.62
P	–	Cr_2O_3	0.03	TiO_2	1.09	TiO_2	1.79
K	–	V_2O_5	0.02	Na_2O	1.89	Na_2O	0.97
Si	–	TiO_2	0.04	MnO	0.20	MnO	0.33
–	–	SO_3	0.45	SO_3	0.09	CuO	0.40
–	–	–	–	P_2O_5	0.07	P_2O_5	0.18
–	–	–	–	ZrO_2	0.04	ZrO_2	0.13
–	–	–	–	NiO	0.04	Cr_2O_3	0.06

area analyzer. The chemical composition of IPC was measured on a Shimadzu X-ray fluorescence (XRF)-1800 with Rh radiation. X-ray diffraction (XRD) was performed using a Rigaku powder diffractometer with Cu K radiation. The tube voltage was 40 kV and the current was 100 mA. XRD diffraction patterns were measured within the range of 10–70℃ at a scan speed of 4° min^{-1}. Phase identification (Search-Match) was carried out in comparison with Joint Committee of Powder Diffraction Standards (JCPDS). Elemental analysis of sawdust was carried out in a VARIO EL III analyzer (Elemental Analysis System Co. Ltd, Germany). As shown in Fig. 1, the compressive strength of IPC was analyzed by using an INSTRON KC-2A material testing machine (China).

The thermal behavior of samples was examined using an EXSTAR simultaneous DTA–TGA 7300 analyzer, while the samples were heated at a rate of 8℃/min from 30–800℃ under a 100 mL/min O_2 atmosphere. Samples ranged from 4–10 mg in mass, and were compacted into a Pt–Rh crucible with 20 taps.

For the analysis of biological structures, IPC and CC were gilt with pores and their surface morphologies were examined using a Scanning Electron Microscope (SEM, Philips XL30 ESEM). The physical characteristics of the IPC were measured in accordance with the sandstone pore structure method of image analysis [29,30]. Microscopic observation of the protozoan and metazoan population was carried out using a U-RFL-T Olympus Biological Microscope (Olympus Corporation, Tokyo, Japan).

2.3. Description of BAF and components of IPC and CC

BAFs were constructed out of a PVC pipe with a 60-mm diameter and length of 1,700 mm. Two BAFs were constructed by packing two pipes with IPC and CC, respectively. Raw wastewater was pumped into the bottom of each BAF with peristaltic pumps and allowed to flow upward through the filter media layer.

2.4. Operation of the experimental BAFs

The operation of the two BAF reactors involved start-up phases that necessitated determination of the parameters compatible with steady-state conditions, approximately 60 d after the start of reactor operation.

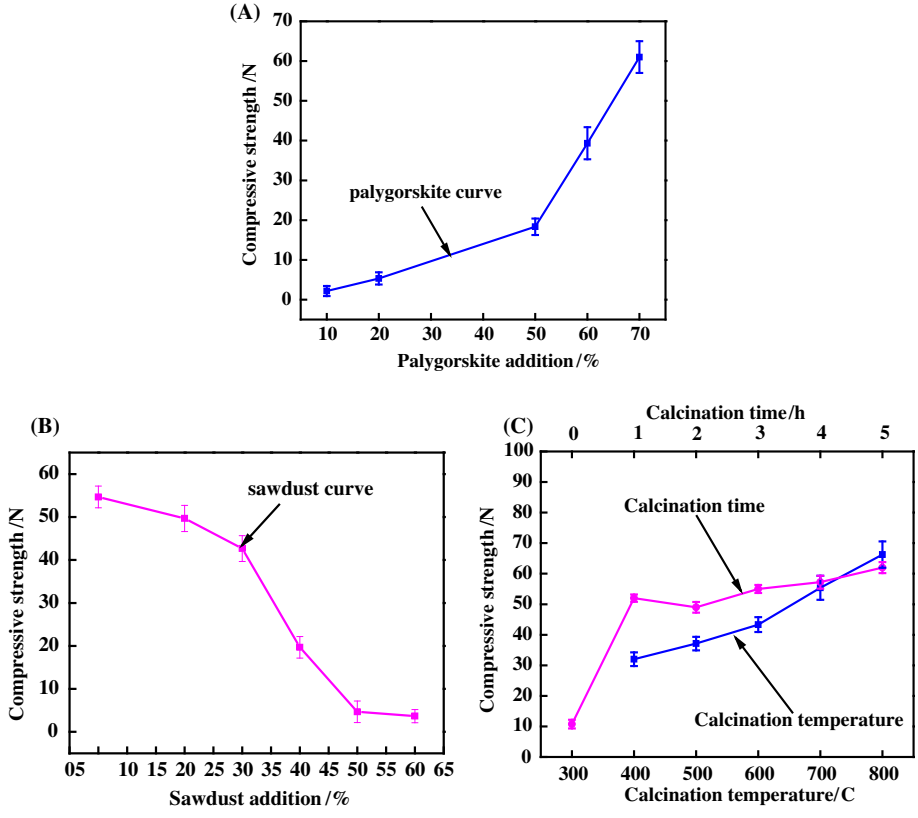

Fig. 1. Effects of IPC preparation. (A) Effect of palygorskite clay on compressive strength of IPC, (B) effect of sawdust on compressive strength of IPC, and (C) IPC compressive strength as a function of calcination temperature and time.

Before the experiments, seed sludge from the Hefei City wastewater treatment plant was inoculated into each BAF reactor. The operating conditions of the two BAFs were identical during start-up (summarized in Supplementary material Table S1). Wastewater samples were collected from the inlet and outlet pipes of the two BAFs. All wastewater samples were stored at 0 ℃ for less than 24 h before analysis. Chinese EPA standard methods were used for chemical determinations [31]. A total organic carbon (TOC)/TN (Jena Multi N/C 2100) analyzer was used to measure TOC and TN. A colorimetric method was used for NH_3-N and phosphorous (P) determinations [31]. DO concentrations were measured using a portable digital DO meter (Oxi-315, China). All chemical reagents were of analytical grade and purchased from the Hefei Chemical Reagent Corporation (China).

3. Results and discussion

3.1. Palygorskite clay content and IPC compressive strength

Compressive strength is an important characteristic of IPC. Fig. 1(A) shows the effect of palygorskite clay content on IPC compressive strength. As the content of palygorskite clay increased from 10 to 50 wt%, the compressive strength increased by 16 N (2 → 18 N). As the content of palygorskite clay increased from 50 to 70 wt%, the compressive strength increased by 43 N (18 → 61 N). Increasing the content of palygorskite clay improved the compressive strength of IPC. The concentration of SiO_2 (≥63.30 wt%) and Al_2O_3 (≥8.35 wt%) (Table 1) suggests that the content and texture of palygorskite clay plays an important role in determining compressive strength. Xu and Zou et al. reported that the substitution of Al^{3+} for Si^{4+} in IPC during the sintering of composite particles, had an effect on the structure, surface physicochemical properties, and thermal stability of composite particles [27,28,32]. We considered 50–70 wt% palygorskite clay content to be the optimal range for production of IPC (Fig. 1(A)).

3.2. Sawdust content and IPC compressive strength

IPC decreased in compressive strength as the amount of sawdust increased (Fig. 1(B)). When sawdust content increased from 5 to 20 wt%, the compressive strength decreased by 6 N (54 → 49 N). Increasing the sawdust content from 20 to 60 wt% was associated with a dramatic decrease in the compressive strength, from 49 to 3 N. Compressive strength of IPC was inversely related to the amount of sawdust content. Several reactions occur in the 400–800 ℃ range (Fig. 5). Sawdust can react with carbon to generate CH_4, CO_2, H_2, and CO [26]. These gases can diffuse or expand through the interior of the IPC, decreasing its compressive strength [33,34].

3.3. Calcination temperature and IPC compressive strength and specific surface area

Fig. 1(C) shows the effect of calcination temperature on IPC compressive strength. An increase in the calcination temperature from 400 to 800 ℃ was associated with a linear increase in compressive strength from 32 to 66 N. The compressive strength increased by 11 N (55 → 66 N) as the calcination temperature increased from 700 to 800 ℃. It has been shown that during the sintering process of goethite from 250 to 700 ℃, the internal and external voids among illusionary goethite particles decrease due to the transformation to hematite particles. The specific surface area of hematite decreased by 94.6 m^2/g (97.4 → 2.8 m^2/g) at >750 ℃ [35]. It has also been shown that palygorskite clay fibers are curved in shape during sintering at 800–1,000 ℃, where the structure changes from a crystalline to an amorphous shape [36–38]. These findings promote optimal IPC performance.

3.4. Calcination time and IPC compressive strength

Calcination time profoundly affected the properties of the IPC product. Fig. 1(C) shows that the compressive strength increased by 51.23 N (10.77 → 62 N) as calcination time increased from 0 to 5.0 h. The IPC compressive strength reached 55 N at about 3 h of calcination time. There were only slight increases in compressive strength as calcination time was extended from 3 to 5 h. Excessive calcination times (>3 h) caused the internal gas pressure to increase, contributing to loss of gas in the material and damage to the internal microporous structure [38].

3.5. Experimental optimization

To assess the effects of palygorskite clay content, sawdust content, calcination temperature, and calcination time on IPC production, the system was optimized with respect to these four factors. An orthogonal $L_9 4^3$ test was used for the optimization of IPC preparation conditions. (Tables S2 and S3) (Supplementary material) Three levels were chosen for each factor to cover a wide range of variation on the basis of the results obtained from the investigations described above (Section 3.1 → Section 3.4). These factors and their levels are shown in Tables S2 and S3.

Table 2
Characteristics of IPC and CC

Item	IPC experimental levels	CC experimental levels
Grain diameter (d, mm)	3–6	0.5–9.0
Silt carrying capacity (C_s, %)	0.15	≤1
Solubility in hydrochloric acid (C_{ha}, %)	1.25	≤2
Void fraction (υ, %)	79.28	≥40
Specific surface area (S_w, cm^2/g)	7.9×10^5	$\geq 0.5 \times 10^4$
Piled density (ρ_p, g/cm^3)	0.523	–
Apparent density (ρ_{ap}, g/cm^3)	1.734	–
Compression strength (N)	51–78	–
Porosity (P, %)	40.5–64.3%	–

The L943 orthogonal evaluation consisted of nine experiments (Tables S2 and S3). The most profound effect on the system was found with variation in sawdust ratio. The second most important factor was calcination time, followed by palygorskite clay ratio and calcination temperature. Goethite was prepared using 100 g of sawdust to a final concentration of 20 wt%, 50 wt% palygorskite clay, a calcination temperature of 700°C, and a calcination time of 180 min. The characteristics of different IPC and CC compositions are shown in Table 2 [39].

3.6. X-ray diffraction (XRD)

Fig. 2(A) and (B) show the XRD patterns of composite particles (as-synthesized IPC) and IPC. The main mineral components of the composite particles were palygorskite, goethite, and quartz (Fig. 2(A)). The characteristic diffraction peaks of palygorskite were completely absent from IPC (Fig. 2(B)). Collapse of the pore structure, loss of crystal structure, and an amorphous structure were observed by XRD in IPC [4]. The characteristic diffraction peaks of goethite were completely absent from IPC. The characteristic reflection intensity of hematite showed a dramatic increase with temperature (700°C, 3 h) because of the increase in crystal size and improvement of crystallinity in newly formed hematite [40,41]. Fig. 2(C) shows the XRD patterns of CC. The strong reflections that appeared at $2\theta = 26^\circ$ were compared to standards (JCPDS 89-6538) and identified as quartz. The main mineral components of the composite particles were hematite and quartz.

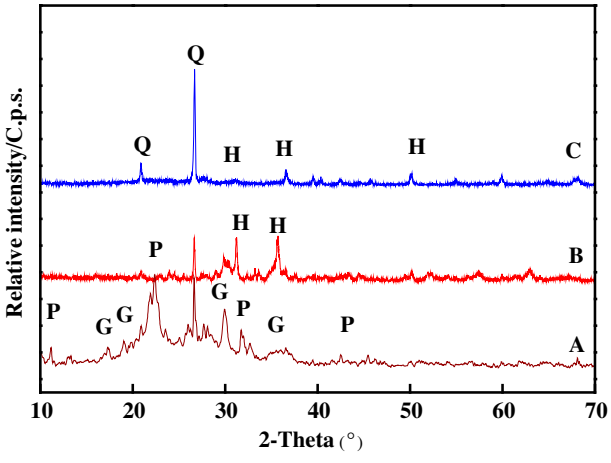

Fig. 2. XRD patterns of as-synthesized IPC (composite particles), IPC, and CC. (A) As-synthesized IPC (composite particles), (B) IPC, and (C) CC; (P-Palygorskite clay; Q-Quartz; M-Magnetic; H-Hematite; G-Goethite).

3.7. XRF and elemental analysis (EA)

The chemical composition of sawdust was C 46.09%, H 6.85%, O 35.09%, N 0.6%, and S 0.1% (EA, Table 1). The majority of CC consisted of SiO_2 (60.24%), Al_2O_3 (17.94%), and Fe_2O_3 (13.16%). Transitional metals (Cr_2O_3 and MnO), alkali and alkaline-earth metal oxides (CaO, MgO, K_2O, and Na_2O, 4.5% in total) were also found in small amounts. Palygorskite clay and goethite served as additives in this study and were used to adjust the chemical composition of IPC. The chemical composition of palygorskite clay, SiO_2 (63.30%), Al_2O_3 (8.35%) and alkali and alkaline-earth metal oxides (17.97%) (Table 1) was significantly higher than that of goethite. The addition of palygorskite clay was found to control the concentration of SiO_2, Al_2O_3, and alkali and alkaline-earth metal oxides in IPC. The preparation of IPC should contain three components [42–46]: (1) glassy materials of SiO_2 and Al_2O_3 from palygorskite clay which is the basic ingredient of IPC and forms the IPC frame work; (2) sawdust and goethite to generate gaseous bubbles of carbon, ferric oxide, ferrous oxide, contributing to pore formation, and (3) flux oxides from goethite and

palygorskite, including CaO, MgO, Na_2O, Fe_2O_3, and MnO, in order to lower the melting point of the glassy phase.

3.8. Scanning electron microscopy (SEM)

The porous structure and biomass growth of IPC and CC were evaluated with SEM (Fig. 3). IPC had a surface pore diameter of 2–500 μm (Fig. 3(A)). There were a large number of macropores on the surface of the IPC which could support micro-organism colonization. These properties made IPC suitable as a filter material for support media. SEM of IPC was performed after BAF operation. Two morphologies of bacteria were observed on the surface of the IPC: filamentous and chain (Fig. 3(B)). CC was found to have a smooth surface (Fig. 3(C)). The morphology of the microstructure suggests that a small number of micro-organisms were immobilized on the outer surfaces of the pores in CC (Fig. 3(D)). The rougher surfaces of IPC contained more large pores than CC. These findings suggest IPC is better suited for the immobilization of micro-organisms.

3.9. Thin-section IPC

The choice of biofilm carrier is key to ensuring the success of nitrogen and phosphorus removal in BAFs. The uneven distribution of DO and substrate inside the IPC's pores and on its rough surface allows simultaneous proliferation of nitrifying and denitrifying bacteria [47]. Rubber casting experiments were used to generate quantitative size and shape data from pores in the thin section in order to obtain more direct examination of micro-organisms between the pores of the IPC [29,30]. The intergranular pores were examined using thin section studies (Fig. 4(A) and (B). The dark red sections denoted calcined palygorskite clay, calcined goethite (hematite), and calcined sawdust residues (biomass carbon). The gray areas represented the intergranular pores of IPC. The size of those interconnected pores was approximately 100–500 μm

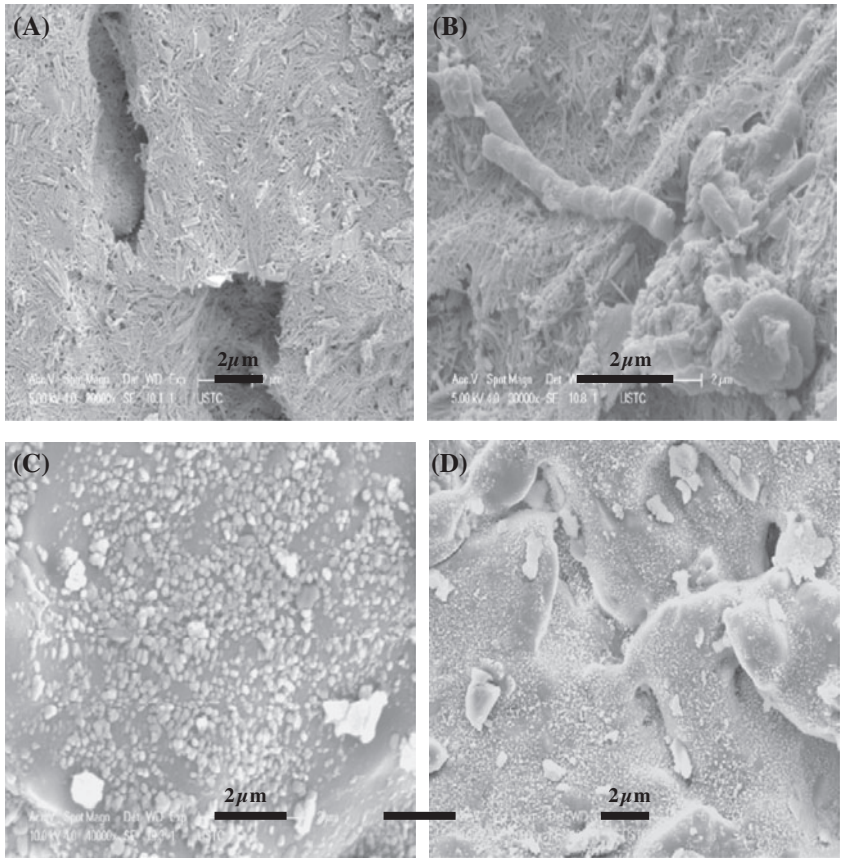

Fig. 3. SEM images of internal and external surface in IPC and CC. (A) Raw external surface of IPC, (B) microbial load on external surface of IPC, (C) raw external surface of CC, and (D) microbial load on external surface of CC.

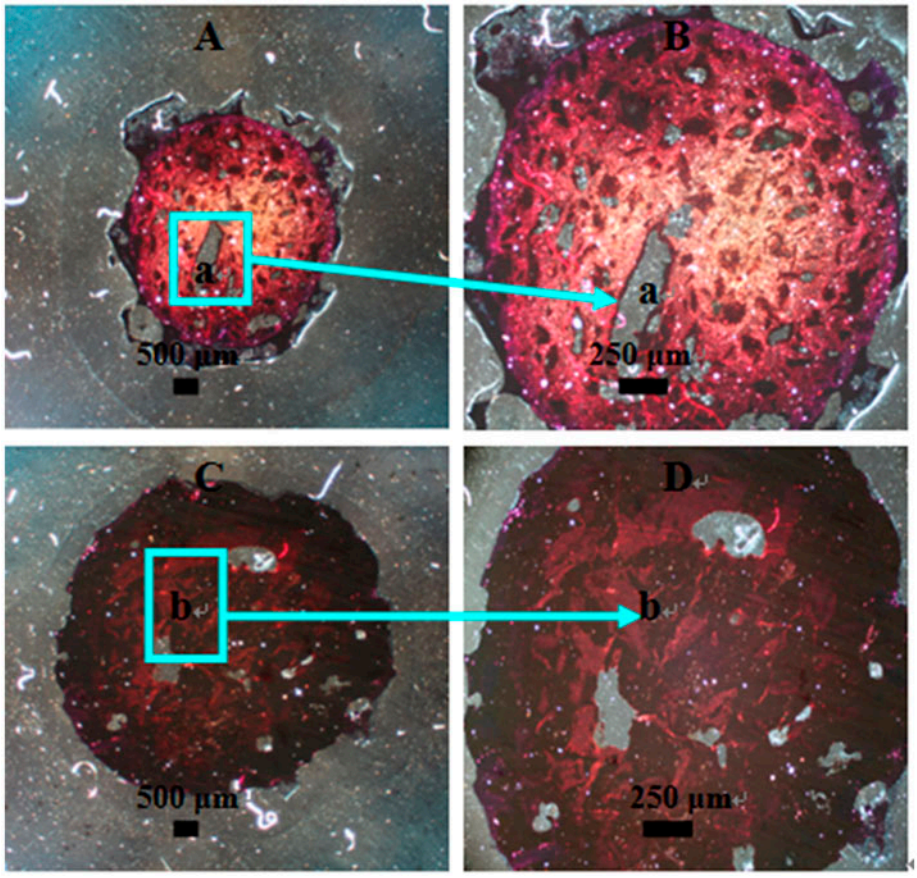

Fig. 4. Porosity of IPC. (A) After calcination (red—IPC), (B) high-resolution image of the internal surface of the IPC, (C) filled (dark red—open pores), and (D) high-resolution image of the internal surface of the IPC (dark red—open pores).

(Fig. 4(C) and (D)). Most bacteria are 0.5 μm or less in diameter. IPC had a large total volume of internal open pores in which guest microbes could be accommodated. The micro-organisms which support the BAF achieved sustained growth in the open pores. The roughness and porosity of the open IPC surface contributed to micro-organism adherence on its surface. The IPC was then impregnated with red-dyed epoxy (part B). Interconnected pores with a diameter of 100–500 μm were identified (part A). The red-dyed epoxy in the pores had to overcome capillary resistance at the pore entrance in order to enter the pores, indicating that the pores were narrow.

4. Thermal properties (DT-TG)

The thermal behavior of raw palygorskite clay, goethite, and sawdust was examined using DTG–TGA. Thermogravimetry (TG) and derivative thermogravimetry (DTG) curves of goethite were characterized (Fig. 5(A)). There was an 11.72% decrease in total mass as the material was heated from 30 to 800˚C. The use of TG and DTG suggest that the weight loss consisted of three components, water loss, dehydroxylation, and loss of residual hydroxyl units. The first mass loss event (1.32%) occurred as the temperature increased from 30 to 230˚C and was due to desorption of adsorbed water bound by hydrogen bonding [35,40]. The second mass loss event (8.72%) occurred as the temperature was increased from 230 to 308˚C. It was attributed to dehydroxylation that occurs with the transformation of goethite to hematite ($2FeOOH \rightarrow Fe_2O_3 + H_2O$). This dehydroxylation was attributed to structural hydroxyl units in goethite. The third mass loss event (1.68%) occurred as the temperature increased from 308 to 800˚C. This loss was attributed to the decomposition of residual structural hydroxyl groups and nonstoichiometric hydroxyl units [35,40].

Absorbed water on the surface and in the channels of palygorskite clay was lost at 70.8 and 155.2˚C, respectively (Fig. 5(B)). However, the structure and morphology of the palygorskite clay remained unchanged at that these temperatures. Some of the water in the palygorskite clay was lost at 203˚C,

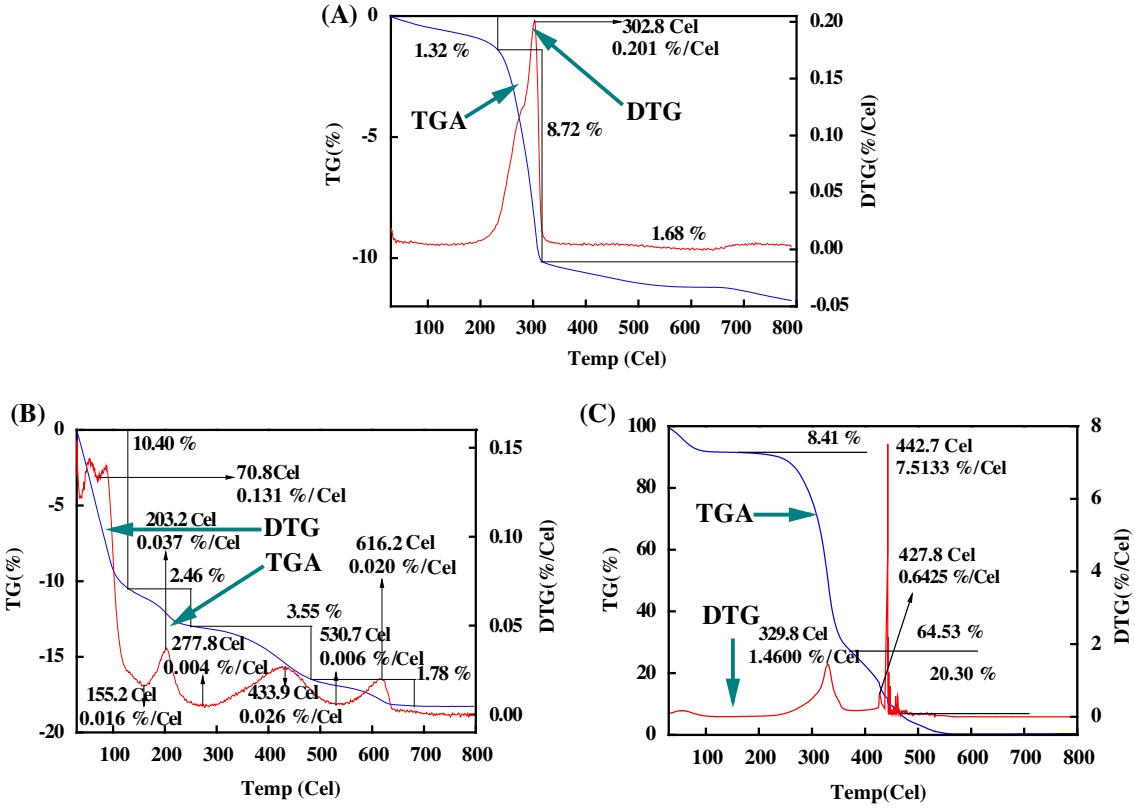

Fig. 5. Differential thermal analysis and thermogravimetric analysis patterns of goethite, palygorskite clay, and sawdust. (A) Goethite, (B) palygorskite clay, and (C) sawdust.

resulting in a structural folds in the clay. Residual water in the palygorskite clay was lost at 433.9℃ and hydroxyls groups were lost at 530.7℃. The channel structure was degraded with these temperature increases, but the ribbon-like structure and morphology of palygorskite clay were not. The morphology of palygorskite clay fibers became curved after treatment at temperatures exceeding 800℃ and the structure changed from crystalline to amorphous [37].

Thermogravimetry (TG) and DTG curves of sawdust were characterized (Fig. 5(C)). 93.24% of the total mass was lost as the temperature increased from 30 to 800℃, The TG and DTG curves suggest this loss took place in three steps. Loss of adsorbed water (8.41%) was observed from 30 to 329.8℃ on the TG curve as gaseous components of the sawdust were lost. The second loss (64.53%) was attributed to the emergence of biomass carbon as the sawdust was heated from 329.8 to 427.8℃. This loss was caused by the dehydration reaction: $3(C_6H_{10}O_5) = 8H_2O + C_6H_8O + 2CO\uparrow + 2CO_2\uparrow + CH_4\uparrow + H_2\uparrow + 7C$. The third loss (20.30%) of mass was seen in the DTG curve as the sawdust was heated from 427.8 to 442.7℃. This loss was attributed to the decomposition of carbon materials by the reaction $C + O_2 \rightarrow CO_2$ [48].

4.1. Influent and effluent BAF concentrations. Removal of TOC, NH_3-N, TN, and P

The IPC BAF and CC BAF achieved a steady state within 60 d of bacteria seeding. City wastewater with 25.84 mg L^{-1} influent and DO concentration >4.00 mg/L was processed in each BAF using a hydraulic retention time of 7 h. TOC removal with the IPC BAF (67.92%) was slightly better than that with the CC BAF (60.71%) (Fig. 6(A)). This might be because of the higher porosity of IPC (40.5–64.3%). The efficiency of TOC removal with the IPC BAF was primarily dependent on the accumulation of activated biofilm on IPC and associated mass transfer efficiency [49]. The average concentrations of influent TN and NH_3-N were 13.96 and 10.51 mg L^{-1}, respectively, during the first 60 d after initial bacteria solution seeding (Fig. 6(B) and (C)). The average removal efficiency of NH_3-N and TN with the IPC BAF was 90.71 and 43.15%, respectively. The average removal efficiency

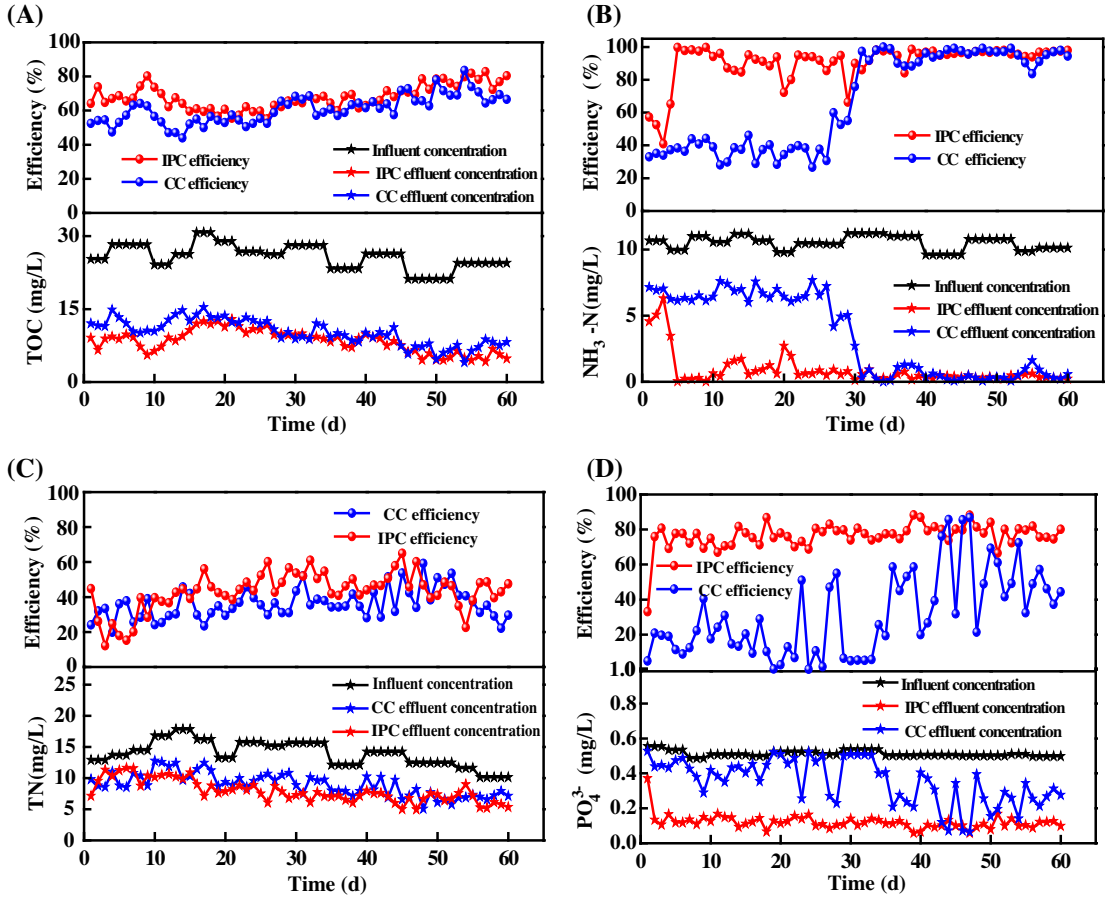

Fig. 6. Influent and effluent concentration and removal efficiency of (A) TOC, (B) NH_3-N, (C) TN, and (D) PO_4^{3-} over time.

of NH_3-N and TN with the CC BAF was 63.96 and 35.96%, respectively.

The biochemical reactions in the biofilms formed anoxic zones as the locally available oxygen was depleted. Biofilm microenvironments with depleted DO and adequate substrate concentrations supported the growth of anaerobic micro-organisms, contributing to simultaneous nitrification–denitrification (SND) in the IPC BAF [50,51]. CC was composed of shale, fly ash, and raw clay and the CC BAF was created by sintering at temperatures greater than 1,200℃. The surface thus had poor hydrophilicity and biocompatibility, decreasing the affinity of its biofilm to the BAF. These findings explain the limited ability of the CC BAF to remove TN. IPC was more suitable as a biofilm carrier than CC. IPC had more open pores and a rougher surface, factors conducive to microbial attachment. The higher specific surface area found with IPC fostered the formation of biological membranes by the adsorbed microorganisms [52–54].

The average removal rates of the CC BAF and IPC BAF 60 d after initial bacterial seeding (steady state) were 32.16 and 76.55%, respectively (Fig. 6(D)). The average influent phosphorus at this time was 0.51 mg/L. Previous studies have shown that nanoscale pores are formed during the transformation of goethite to hematite. The high temperatures used for this process contribute to even more pore formation. The high temperatures also led to complete dehydroxylation with loss of crystal structure, a change from an octahedral to a tetrahedral conformation, and loss of penta coordination. These changes result in an amorphous material. Hematite derived from annealed goethite with micropores and mesopores has a much higher adsorption capacity for phosphate than other substances [10]. One report suggested that calcinated palygorskite clay has the highest adsorption capacity of studied materials. Together, these findings contribute to the increased activity and phosphate adsorption of Al [4].

5. Conclusions

(1) IPC was prepared from a mixture of goethite, sawdust, and palygorskite clay at a weight ratio of 10:2:5. Calcination was performed at 700°C for 180 min in order to produce IPC suitable for wastewater treatment. SEM and porosimetry results suggest the uniform, interconnected pores in IPC were suitable for microbial growth. Sawdust can serve as a pore-forming agent, facilitating the production of ceramisite with interconnected pores.

(2) BAFs consisting of IPC and CC 60 d after startup (steady state) had TOC removal efficiencies of 67.92 and 60.71%, respectively, NH_3-N removal efficiencies of 90.71 and 67.29%, respectively, TN removal efficiencies of 43.15 and 35.96%, respectively, and P removal efficiencies of 76.55 and 32.16%, respectively. IPC showed much better performance than CC. IPC could serve as a medium for micro-organism containment in advanced wastewater treatment systems.

Supplementary material

The supplementary material for this paper is available online at http://dx.doi.10.1080/19443994.2015.1101021.

Acknowledgements

This work was supported by the National Natural Science Foundation of China (41072036, 41130206, 41372045, 41202021), the Specialized Research Fund for the Doctoral Program of Higher Education of China (20110111110003).

References

[1] H.P. Ye, F.Z. Chen, Y.Q. Sheng, Adsorption of phosphate from aqueous solution onto modified palygorskites, Sep. Purif. Technol. 50 (2006) 283–290.
[2] G. Akay, B. Keskinler, A. Cakici, U. Danis, Phosphate removal from water by red mud using crossflow microfiltration, Water Res. 32 (1998) 717–726.
[3] T. Bao, T.H. Chen, C.S. Qing, J.J. Xie, R.L. Frost, Development and application of palygorskite porous ceramsite in a biological aerated filter (BAF), Desalin. Water Treat. (2014) 1–14, doi: 10.1080/19443994.2014.976770.
[4] J.J. Xie, T.H. Chen, C.S. Qing, Adsorption of phosphate from aqueous solutions by thermally modified palygorskite, Environ. Eng. Manage. J. 12 (2013) 1393–1399.
[5] G. Zelmanov, R. Semiat, The influence of competitive inorganic ions on phosphate removal from water by adsorption on iron (Fe^{+3}) oxide/hydroxide nanoparticles-based agglomerates, J. Water Process Eng. 5 (2015) 143–152.
[6] M.M. Benjamin, Water Chemistry, McGraw Hill Higher Education, Singapore, 2002.
[7] L. Zeng, X. Li, J.D. Liu, Adsorptive removal of phosphate from aqueous solutions using iron oxide tailings, Water Res. 38 (2004) 1318–1326.
[8] H.B. Liu, T.H. Chen, R.L. Frost, An overview of the role of goethite surfaces in the environment, Chemosphere 103 (2014) 1–11.
[9] H.B. Liu, T.H. Chen, X.H. Zou, Removal of phosphorus using NZVI derived from reducing natural goethite, Chem. Eng. J. 234 (2013) 80–87.
[10] H.B. Liu, T.H. Chen, J. Chang, The effect of hydroxyl groups and surface area of hematite derived from annealing goethite for phosphate removal, J. Colloid Interface Sci. 398 (2013) 88–94.
[11] J.Y. Shen, R. He, H.X. Yu, Biodegradation of 2,4,6-trinitrophenol (picric acid) in a biological aerated filter (BAF), Bioresour. Technol. 100 (2009) 1922–1930.
[12] J.Q. Sang, X.H. Zhang, L.Z. Li, Improvement of organics removal by bio-ceramic filtration of raw water with addition of phosphorus, Water Res. 37 (2003) 4711–4718.
[13] L. Mendoza-Espinosa, T. Stephenson, A review of biological aerated filters (BAFs) for wastewater treatment, Environ. Eng. Sci. 16 (1999) 201–216.
[14] P. Lai, H.Z. Zhao, Z.F. Ye, Assessing the effectiveness of treating coking effluents using anaerobic and aerobic biofilms, Process Biochem. 43 (2008) 229–237.
[15] Y. Feng, Y.Z. Yu, L.P. Qiu, Performance of water quenched slag particles (WQSP) for municipal wastewater treatment in a biological aerated filter (BAF), Biomass Bioenergy 45 (2012) 280–287.
[16] W.S. Chang, H.T. Tran, D.H. Park, Ammonium nitrogen removal characteristics of zeolite media in a biological aerated filter (BAF) for the treatment of textile wastewater, J. Ind. Eng. Chem. 15 (2009) 524–528.
[17] Z. Li, B.Y. Gao, Q.Y. Yue, Study and application of biological-aerated filter (BAF) in soybean protein advanced wastewater treatment, Desalin. Water Treat. 51 (2013) 3248–3256.
[18] J. Werner, B. Besser, C. Brandes, Production of ceramic membranes with different pore sizes for virus retention, J. Water Process Eng. 4 (2014) 201–211.
[19] Y. Feng, Y.Z. Yu, L.P. Qiu, Domestic wastewater treatment using biological aerated filtration system with modified zeolite as biofilm support, Desalin. Water Treat. 52 (2014) 5021–5030.
[20] Z. Li, B.Y. Gao, Q.Y. Yue, UASB-A/O-BAF treatment of high strength wastewater: A case study for soybean protein wastewater, Desalin. Water Treat. 47 (2012) 24–30.
[21] Y. Feng, Y.Z. Yu, L.P. Qiu, The characteristics and effect of grain-slag media for the treatment of phosphorus in a biological aerated filter (BAF), Desalin. Water Treat. 47 (2012) 258–265.
[22] S.P. Li, J.J. Cui, Q.L. Zhang, Performance of blast furnace dust clay sodium silicate ceramic particles (BCSCP) for brewery wastewater treatment in a biological aerated filter, Desalination 258 (2010) 12–18.

[23] S.X. Han, Q.Y. Yue, M. Yue, Effect of sludge-fly ash ceramic particles (SFCP) on synthetic wastewater treatment in an A/O combined biological aerated filter, Bioresour. Technol. 100 (2009) 1149–1155.
[24] F. Liu, C.C. Zhao, D.F. Zhao, Tertiary treatment of textile wastewater with combined media biological aerated filter (CMBAF) at different hydraulic loadings and dissolved oxygen concentrations, J. Hazard. Mater. 160 (2008) 161–167.
[25] E. Salehi, J. Abedi, T. Harding, Bio-oil from sawdust: Pyrolysis of sawdust in a fixed bed system, Bioresour. Technol. 23(2009) 3767–3772.
[26] G.D. Ji, Y. Zhou, J.J. Tong, Nitrogen and phosphorus adsorption behavior of ceramsite material made from coal ash and metallic iron, Environ. Eng. Sci. 27 (2010) 871–878.
[27] G.R. Xu, J.L. Zou, G.B. Li, Ceramsite made with water and wastewater sludge and its characteristics affected by SiO_2 and Al_2O_3, Environ. Sci. Technol. 42 (2008) 7417–7423.
[28] G.R. Xu, J.L. Zou, Y. Dai, Utilization of dried sludge for making ceramsite, Water Sci. Technol. 54 (2006) 69–79.
[29] Measurement of Sandstone pore structure method of image analysis (SY/T6103-004), Oil and Natural Gas Industry Standards of the People's Republic of China (in Chinese).
[30] K. Ruzyla, D.I. Jezek, Staining method for recognition of pore space in thin and polished sections, J. Sediment. Res. 57 (1987) 777–778.
[31] Chinese EPA, Methods for Water and Wastewater Analysis, fourth ed., Environmental Science Publishing House of China, Beijing, 2002.
[32] Y.J. Park, J. Heo, Vitrification of fly ash from municipal solid waste incinerator, J. Hazard. Mater. 91 (2001) 83–93.
[33] C.M. Riley, Relation of chemical properties to the bloating of clays, J. Am. Ceram. Soc. 34 (1951) 121–128.
[34] S.C. Huang, F.C. Chang, S.L. Lo, Production of lightweight aggregates from mining residues, heavy metal sludge, and incinerator fly ash, J. Hazard. Mater. 144 (2007) 52–58.
[35] X.H. Zou, T.H. Chen, H.B. Liu, Structural and chromatic evolution of goethite by thermal treatment, J. Chin. Chem. Soc. 41 (2013) 669–673.
[36] H.B. Liu, T.H. Chen, D.Y. Chang, The difference of thermal stability between Fe-substituted palygorskite and Al-rich palygorskite, J. Therm. Anal. Calorim. 111 (2013) 409–415.
[37] T.H. Chen, J. Wang, C.S. Qing, Effect of heat treatment on structure, morphology and surface properties of palygorskite, J. Chin. Chem. Soc. 34 (2006) 1406–1410.
[38] T. Bao, T.H. Chen, H.B. Liu, Preparation of magnetic porous ceramsite and its application in biological aerated filters, J. Water Process Eng. 150 (2014) 394–400.
[39] C. Mohurd, Artifical Ceramsite Filter Material for Water Treatment, China Standard Publishing House, Beijing, 2008.
[40] H.B. Liu, T.H. Chen, X.H. Zou, Thermal treatment of natural goethite: Thermal transformation and physical properties, Thermochim. Acta 568 (2013) 115–121.
[41] R.L. Frost, Z. Ding, H. Ruan, Thermal analysis of goethite relevance to Australian indigenous art, J. Therm. Anal. Calorim. 71 (2003) 783–797.
[42] A. Fullana, J.A. Conesa, R. Font, Formation and destruction of chlorinated pollutants during sewage sludge incineration, Environ. Sci. Technol. 38 (2004) 2953–2958.
[43] S.Q. Wu, Y.F. Qi, Q.Y. Yue, Preparation of ceramic filler from reusing sewage sludge and application in biological aerated filter for soy protein secondary wastewater treatment, J. Hazard. Mater. 283 (2015) 608–616.
[44] C.C. Tsai, K.S. Wang, I.J. Chiou, Effect of SiO_2–Al_2O_3-flux ratio change on the bloating characteristics of lightweight aggregate material produced from recycled sewage sludge, J. Hazard. Mater. 134 (2006) 87–93.
[45] J.A. Cusidó, L.V. Cremades, M. González, Gaseous emissions from ceramics manufactured with urban sewage sludge during firing processes, Waste Manage. 23 (2003) 273–280.
[46] K.J. Mun, Development and tests of lightweight aggregate using sewage sludge for nonstructural concrete, Constr. Build. Mater. 21 (2007) 1583–1588.
[47] J.L. Zou, G.R. Xu, K. Pan, Nitrogen removal and biofilm structure affected by COD/NH_4^+–N in a biofilter with porous sludge-ceramsite, Sep. Purif. Technol. 94 (2012) 9–15.
[48] C.P. Wang, F.Y. Wang, Q.R. Yang, Thermogravimetric studies of the behavior of wheat straw with added coal during combustion, Biomass Bioenergy 33 (2009) 50–56.
[49] L.P. Qiu, S.B. Zhang, G.W. Wang, Performances and nitrification properties of biological aerated filters with zeolite, ceramic particle and carbonate media, Bioresour. Technol. 101 (2010) 7245–7251.
[50] K.A. Third, B. Gibbs, M. Newland, Long-term aeration management for improved N-removal via SND in a sequencing batch reactor, Water Res. 39 (2005) 3523–3530.
[51] Y.C. Chiu, L.L. Lee, C.N. Chang, A.C. Chao, Control of carbon and ammonium ratio for simultaneous nitrification and denitrification in a sequencing batch bioreactor, Int. Biodeterior. Biodegrad. 59 (2007) 1–7.
[52] J. Zhang, X. Huang, C.X. Liu, Nitrogen removal enhanced by intermittent operation in a subsurface wastewater infiltration system, Ecol. Eng. 25 (2005) 419–428.
[53] S. Luostarinen, S. Luste, L. Valentín, Nitrogen removal from on-site treated anaerobic effluents using intermittently aerated moving bed biofilm reactors at low temperatures, Water Res. 40 (2006) 1607–1615.
[54] L.W. Xiao, M. Rodgers, J. Mulqueen, Organic carbon and nitrogen removal from a strong wastewater using a denitrifying suspended growth reactor and a horizontal-flow biofilm reactor, Bioresour. Technol. 98 (2007) 739–744.